Using Physical Modeling and RGB-D Registration for Contact Force Sensing on Deformable Objects

Antoine Petit[1], Fanny Ficuciello[1], Giuseppe Andrea Fontanelli[1], Luigi Villani[1] and Bruno Siciliano[1]
[1]*Dipartimento di Ingegneria Elettrica e Tecnologie dell'Informazione,*
Università degli Studi di Napoli, via Claudio 21, 80125 Napoli, Italy
$\{$*antoine.petit, fanny.ficuciello, giuseppeandrea.fontanelli, lvillani, siciliano*$\}$*@unina.it*

Keywords: Force Estimation, Physical Modelling, Deformable Objects

Abstract: In this paper we propose a method to estimate the force applied to a manipulated deformable object by processing information provided by an external vision sensor, in this case a consumer RGB-D camera. By measuring the deformations undergone by the object through a registration technique, the idea is to retrieve the contact force which minimises the deviation between the measured and the simulated deformations, given a simple interaction model and by employing a fitting process. The system resorts to a realistic mesh-based Finite Element Method model to accurately model deformations, whose elastic parameters are estimated in advance using the vision system and a force sensor. Experimental results are presented for the case of a compressive point-wise contact force applied, at static equilibrium, on a deformable object.

1 INTRODUCTION

The measure of contact forces is a key requirement in various applications such as capturing and synthesising human manipulation tasks or controlling robotic hands. Force sensing for robotics or virtual reality applications is typically based on mechatronic transducers (Siciliano and Khatib, 2008; Fazioli et al., 2016). These devices can be placed on the object to be manipulated, or on the operator, embedded on skins or gloves (Wettels et al., 2009; Dahiya et al., 2010; Yousef et al., 2011; Cirillo et al., 2015). Force can be also estimated through sensing devices mounted on the joints of the robot manipulator. However, in applications as minimally invasive surgery, these sensors cannot be easily installed on surgical instruments, due to the need of sterilisation or electrification.

Capturing the interactions in manipulation based on computer vision has aroused considerable interest recently and may represent a convenient, minimally invasive and cheap sensing set-up. Some efforts have been focused on sensing the interactions between rigid objects, but the field remains open when considering deformations.

The main contribution of this paper is to propose a method enabling to measure contact forces between the operator and a deformable object, using an RGB-D camera. The task is very challenging, since a given deformation can be gendered by a multiplicity of interactions. Here we demonstrate that, by confronting a physical deformation model for the object with deformations measured through vision, it is possible to retrieve a single point-wise contact force exerted by an operator (a human hand, a robot end-effector) on the considered object. The material properties of the object, consisting in elastic parameters, are estimated in a preliminary step by using a force sensor and an optimisation technique. Then, assuming that the object lies on a flat surface and that the tool/object interaction consists in a known single contact point, a similar optimisation technique is used to infer the value of the 3D force exerted on that point. This is achieved by fitting the simulated deformations with those measured by the vision system. The proposed approach is based on the techniques suggested in (Petit et al., 2015b; Petit et al., 2017).

1.1 Related Works

Approaches using visual information as a cue to measure contact force have recently appeared. For instance in (Hristu et al., 2000; Mascaro and Asada, 2001; Sun et al., 2008; Sun et al., 2009; Urban et al., 2013; Grieve et al., 2013; Essahbi et al., 2015), the changes in the appearance of the fingertip are measured through photodetectors or an external camera, and are processed to estimate contact forces using statistical models. These techniques are limited to measure the normal force and cannot simultaneously consider shear or slip. A promising approach (Yuan et al., 2015), also based on visual observations, relies on the GelSight sensor (Sato et al., 2010). In this case the deformations, measured by marker-based visual tracking techniques on an embedded elastomer medium, are interpreted as known responses to the external load exerted on the sensor.

All the above force sensing methods require instrumenting the interacting tool/hand and/or the manipulated object with cumbersome and expensive equipment which can also limit the range of motion. Often they are tailored to particular objects and hard to generalise, whereas we wish to design a generic data-driven system. Force sensing based on an external sensing device represent an appealing alternative and vision sensors appear as the most simple, cheap, convenient technology to propose.

Several works in the literature have suggested the use of an external vision system to capture the interactions and to sense contact forces in the case of object manipulation by a human or any manipulation tool. In the motion capture field, this approach has been investigated by some systems using marker-based or markerless vision tracking to capture and synthesise hand/object interaction (Oikonomidis et al., 2011; Ballan et al., 2012; Kyriazis and Argyros, 2013). A kinematic analysis of the interactions through discriminative or generative processes is performed and some physics-based constraints are introduced to deal with occlusions or collision detection. Some other approaches (Wang et al., 2013; Zhao et al., 2013) propose to bridge the gap between the kinematics provided by the motion capture systems and the contact forces by linking physical constraints to visual observations.

The techniques proposed in (Brubaker et al., 2009; Pham et al., 2015) go further by employing rigid body and contact dynamics to fully model interactions, and to link these models with the kinematics provided by an external vision systems. In this way the contact forces between a human and the ground (Brubaker et al., 2009) or between a hand and a manipulated object (Pham et al., 2015; Ficuciello et al., 2010) can be estimated in a physically realistic manner. To the best of our knowledge, these are the only works proposed in the literature where external visual tracking is used as a cue for contact force estimation, in the case of rigid and articulated bodies interactions.

1.2 Contribution

In this paper we propose to use an external vision system to infer contact forces deriving from the manipulation of deformable objects, by confronting the physical properties of the object and its deformation model with the output of the vision system. Our approach is close to the idea in (Yuan et al., 2015) of relating measured deformations to forces. The method presented in (Yuan et al., 2015), however, relies on an embedded sensing device and addresses force estimation through empirical relationships between deformations and forces.

In our approach, as major contribution, we propose to use realistic physical modeling of a deformable object to infer interaction forces exerted on it, by processing external vision data. We focus here on a static case. The general idea is to estimate a point-wise contact force for which the resulting deformations best fit the deformations measured by the vision system. We assume the contact point to be known and the deformable object to be isotropic.

Relying on a physical model implies knowing the mechanical properties of the object. Here we employ the Finite Element Method (FEM) to model the object and its elasticity, which is described by two parameters, the Young Modulus and the Poisson ratio. As a second contribution, we suggest to estimate these two parameters during a preliminary step. Conversely to the force estimation process, a force sensor is used in order to fit the simulated deformations based on the measured contact force with the vision data.

2 DEFORMATION AND INTERACTION MODELS

A key issue of this work is to rely on a realistic physical deformation model of the considered elastic and isotropic object. A FEM model provides accurate physical realism, by relying on continuum mechanics, instead of finite differences for mass-spring systems for instance. For an exhaustive description of FEM, the reader can refer to (Cook, 1994). The method consists in tessellating the deformable object into a mesh made of elements connecting a set $X = \{\mathbf{x}_j\}_{j=1}^{nX}$ of 3D vertices. The deformation fields over the elements are approximated as continuous interpolations of the displacements of the vertices. We rely here on a volumetric linear FEM approach with tetrahedral elements.

2.1 Modeling Elastic Deformations

In order to model elasticity for a continuous isotropic material, we follow the method proposed in (Petit et al., 2015a), by resorting to the linear elasticity, with Hooke's law, and to the infinitesimal strain theory (Cook, 1994), modified by adopting a co-rotational approach (Etzmuß et al., 2003; Müller and Gross, 2004; Nesme et al.,), so as to accommodate to rotation transformations. The infinitesimal strain tensor ε_e and stress tensor σ_e within a tetrahedron e can be written using the Voigt notation in terms of 6×1 vectors as:

$$\varepsilon_e = \mathbf{L}_e \hat{\mathbf{u}}_e^r = \mathbf{L}_e(\mathbf{R}_e^{-1}\mathbf{x}_e - \mathbf{x}_{e,0}) \quad (1)$$
$$\sigma_e = \mathbf{C}_e(E, \nu)\varepsilon_e.$$

If the deformations $\hat{\mathbf{u}}_e$ can be written as $\hat{\mathbf{u}}_e = \mathbf{x}_e - \mathbf{x}_{e,0}$, we define here $\hat{\mathbf{u}}_e^r = \mathbf{R}_e^{-1}\mathbf{x}_e - \mathbf{x}_{e,0}$, with $\mathbf{R}_e^{-1}\mathbf{x}_e$ the back rotated deformed coordinates of the four vertices of e, stacked into the 12×1 vector $\mathbf{x}_e$. $\mathbf{R}_e$ is a 12×12 block diagonal matrix containing four copies of the 3×3 rotation matrix corresponding the rotational component of the deformations of the element. $\mathbf{L}_e$ is the constant 6×12 matrix related to the interpolation function, $\mathbf{C}_e$ is a 6×6 symmetric matrix depending on two elastic parameters of the material, the Young modulus E and the Poisson ratio ν.

The internal elastic forces $\mathbf{f}_e$ exerted on the vertices of e can then be related to $\hat{\mathbf{u}}_e^r$ through:

$$\mathbf{f}_e = \mathbf{R}_e \mathbf{K}_e \hat{\mathbf{u}}_e^r \quad (2)$$

being $\mathbf{K}_e = V_e \mathbf{L}_e^T \mathbf{C}_e \mathbf{L}_e$ the stiffness matrix of the element of volume V_e. In this way, the overall forces on the whole mesh can be summed to zero, while computational efficiency is ensured since $\mathbf{K}_e$ can be computed in advance, in contrast to non-linear FEM approaches.

2.2 Modeling Interaction

We consider the case of a manipulated object lying on a known flat rigid surface. The object is then deformed by a single contact force which acts vertically, so that the contact between the object and the plane remains constant. In the experiments (see Section 6), this force is applied by a tool mounted on a robotic arm. We assume a pointwise contact on a point of known position lying on the surface of the object. Considering for the simulation model the mesh $X = \{\mathbf{x}_j\}_{j=1}^{nX}$, and using the co-rotated deformation model described in Section 2.1, the Lagrangian dynamics is described by the equations:

$$\mathbf{M}\ddot{\mathbf{x}} + \mathbf{C}\dot{\mathbf{x}} + \mathbf{f} = \mathbf{f}_{ext}^{sim} \quad (3)$$
$$\text{with} \quad \mathbf{f}_{ext}^{sim} = \mathbf{M}\mathbf{G} + \mathbf{f}^{ground} + \mathbf{f}^{op}$$

where $\mathbf{G}$ is the vector of the gravity forces applied to the vertices, $\mathbf{f}^{op}$ is the pointwise external force exerted by the operator, and $\mathbf{f}^{ground}$ is the vector of the contact forces of the flat rigid surface or ground, exerted on the vertices in contact with it. These forces act on vertices of the mesh for which the signed distance is negative (below the plane), attracting them thus towards the plane. We simply model them as damped linear springs according to the signed distance between the vertices of mesh and the known plane representing the surface. We assume an inelastic surface, meaning that the stiffness of the springs is set high. For simplicity and since we deal with a vertical compressing effort on the object, we neglect adhesive sticky effects, as well as tangential friction.

3 ESTIMATION OF THE DEFORMATIONS WITH RGB-D DATA

In this section the external vision data is used to estimate, in a physically realistic manner, the deformations undergone by the object which will then drive the estimation of the force exerted by an operator (see Section 5). The registration problem we tackle consists in fitting the point cloud data, provided by an RGB-D sensor, with the tetrahedral mesh, in terms of both rigid and non-rigid transformations. We directly employ the approach proposed in (Petit et al., 2015a), for which the main steps are recalled hereafter:

Preliminary visual segmentation. The visual segmentation step presented in (Petit et al., 2015a) is carried out in order to restrict the acquired point cloud to the considered object, so as to avoid ambiguities in the matching process with the background or with occluding shapes. This phase provides us with the set Y of the 3D points of the target point cloud. We limit the size of Y by sampling $\mathbf{D}^k$ on a regular grid in the image plane.

Rigid iterative closest point. The observed segmented point cloud Y is registered in terms of rigid translation and rotation transformations, initially considering the mesh of the object as rigid. We employ a classical rigid Iterative Closest Point (ICP) algorithm (Chen and Medioni, 1992) between Y and the vertices of the visible surface X_V of the mesh, transformed with respect to the previous RGB-D data. Through this procedure a fair initialization for the non-rigid process can be obtained.

Deformable registration process. Following the approaches in (Petit et al., 2015a; Petit et al., 2015b), the basic idea is to derive external forces exerted by the point cloud on the mesh, and to balance them with the internal forces based on the deformation model presented in Section 2, with respect to the displacements of the vertices of the mesh. In this work, we use external forces $\mathbf{f}_{ext}^{g}$ related to geometrical information as introduced in (Petit et al., 2015a). The method consists first in determining nearest neighbors correspondences, both from the segmented point cloud to

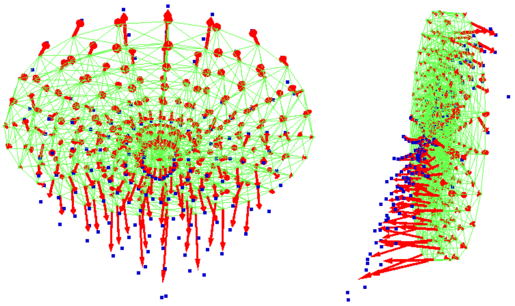

Figure 1: External forces based on nearest neighbours searches.

the mesh and from the mesh to the segmented point cloud, as shown in Fig.1.

Based on the two sets of mesh-to-point cloud and point cloud-to-mesh correspondences, an external elastic force $\mathbf{f}^g_{ext}$ exerted on each $\mathbf{x}_j$ in X_V, can be computed as follows:

$$\mathbf{f}^g_{ext}(\mathbf{x}_j) = k^g_{ext}(\mathbf{x}_j - \mathbf{y}^f_j) \tag{4}$$

where, as described in (Petit et al., 2015a), $\mathbf{y}^f_j$ is a linear combination of points in the point clouds which are matched to $\mathbf{x}_j$, either from mesh-to-point cloud and from point cloud-to-mesh correspondence sets. k^g_{ext} is the stiffness of these external elastic forces.

Estimation. Estimating the deformations of the mesh consists in solving a dynamic system of linear ordinary differential equations involving the internal and external forces, based on the Lagrangian dynamics:

$$\mathbf{M}\ddot{\mathbf{x}} + \mathbf{C}\dot{\mathbf{x}} + \mathbf{f} = \mathbf{f}^g_{ext} \tag{5}$$
$$\text{with} \quad \mathbf{f} = \mathbf{K}\mathbf{x} + \mathbf{f}_0$$

where $\mathbf{x}$ is a $3n_X \times 1$ vector containing the positions to estimate of the vertices in X, $\mathbf{M}$ and $\mathbf{C}$ are the $3n_X \times 3n_X$ mass and damping matrices, $\mathbf{K}$ the $3n_X \times 3n_X$ global stiffness matrix which sums the $3n_X \times 3n_X$ element-wise *rotated* stiffness matrices $\mathbf{K}^r_e = \mathbf{R}_e\mathbf{K}_e\mathbf{R}_e^{-1}$, written with respect to whole set of vertices, and $\mathbf{f}_0$ the corresponding global offset summing the element-wise ones $\mathbf{R}_e\mathbf{K}_e\mathbf{x}_{e,0}$. $\mathbf{f}^g_{ext}$ is a $3n_X \times 1$ vector containing the external forces defined in equation (4).

An Euler implicit integration scheme is used in (Petit et al., 2015a) to solve the system with respect to $\mathbf{x}$, along with a conjugate gradient method. Notice that here we consider the static case, with the static equilibrium of the deformations assumed to be reached, so the transient and the dynamic terms of equation (5) could be neglected, leading to simply solving the equality between internal elastic forces and external forces with the conjugate gradient method.

4 ESTIMATION OF ELASTIC PARAMETERS

The elastic parameters of the object are estimated using the point cloud data on the basis of the deformations observed using an RGB-D sensor, and of the force measurements provided by a force sensor. Notice that this force sensor is used only for this preliminary step, and can be unmounted for the second step where, conversely, the estimation of the contact force is made using vision.

Here we follow the data-driven approaches described in (Frank et al., 2010; Wang et al., 2015). They consist in minimizing a fitting error between the simulated deformations, actuated by the input operator force provided by the sensor, and the deformations captured by the RGB-D sensor. These two methods also employ finite elements for the deformation model. The work (Wang et al., 2015) goes further by proposing a framework that sequentially tracks the shape and estimates both material and dynamic parameters (damping). A dynamic deformation model is used and the vision capture set-up consists in various RGB-D sensors around the scene.

Here we consider a static model and limit this preliminary process to the estimation of the Young modulus and the Poisson ratio of the material. We use a single RGB-D sensor and a force sensor mounted on a robotic arm, with a set-up similar to the one proposed in (Frank et al., 2010). The deformations are indeed generated by applying an effort, in our case compression, on the deformable object and we observe the deformations with the vision sensor once static equilibrium is reached.

These deformations can be simulated, starting from the same initial rest shape, by using the deformation and interaction model presented above and the input measured contact force. Our problem is then addressed by minimizing, with respect to the elasticity parameters, the deviation between these simulated deformations, and the observed ones. This deviation is defined by a fitting function e_{param} accounting for the sum of squared distances between the point cloud acquired on the object, and the simulated deformations, defined as:

$$e_{param}(E,\nu) = dist(sim(E,\nu,\mathbf{f}^{op}(\mathbf{x}_{i_c})),Y) \tag{6}$$

where E and ν are respectively the Young modulus and the Poisson ratio, $\mathbf{f}^{op}$ is the measured contact force exerted by the operator on the object, on the contact point $\mathbf{x}_{i_c}$, Y is the acquired point cloud. We use the point cloud segmented on the considered object by running the segmentation phase described in Sect. 3. For a relevant significant error function, we employ the matching technique presented in Sect. 3 between the segmented point cloud and the visible part of the deformed mesh, and conversely. Based on the two sets of mesh-to-point cloud and point cloud-to-mesh correspondences, the error function is calculated as:

$$e_{param}(E,\nu) = \frac{1}{n_{X_V}} \sum_{i=0}^{n_{X_V}} (\mathbf{x}_i^{sim} - \mathbf{NN}_Y(\mathbf{x}_i^{sim}))^2 + \frac{1}{n_Y} \sum_{j=0}^{n_Y} (\mathbf{y}_j - \mathbf{NN}_{X_V}(\mathbf{y}_j))^2 \qquad (7)$$

where $X_V = \{\mathbf{x}_i^{sim}\}_{i=0}^{n_{X_V}}$ are the vertices of the visible part of the mesh which is deformed by simulation. $Y = \{\mathbf{y}_j\}_{j=0}^{n_Y}$ are the vertices of the segmented point cloud. $\mathbf{NN}_Y(\mathbf{x}_i^{sim})$ and $\mathbf{NN}_{X_V}(\mathbf{y}_j)$ define the correspondences between $\mathbf{x}_i^{sim}$ and $\mathbf{y}_j$, using nearest neighbour searches respectively within the sets Y and X_V. This optimization problem with respect to (E,ν) is non-linear and the evaluation of the objective function is expensive and its gradients are non-trivial to compute making gradient-based optimization methods prohibitive. We thus employ the gradient-free Nelder-Mead method (Nelder and Mead, 1965), which is an extension of the downhill simplex method to the non-linear case. For each evaluation of the objective function in the Nelder-Mead process, the mesh is initially reset to its rest shape. We then apply the measured contact force $\mathbf{f}^{op}$ on the known vertex of the mesh, given the elasticity parameters (E,ν) to evaluate. A simulation is then started until a static equilibrium is reached. From this static equilibrium, the matching process that leads to equation (7) is handled.

5 ESTIMATION OF THE CONTACT FORCE

The problem of computing the contact force exerted on the manipulated object also consists in a fitting procedure between the simulated and the observed deformations. Knowing the material parameters, we can use the deformation model and the registration technique described in Sect. 3, providing a regularized and complete observation of the deformations.

The idea is to determine the force for which the resulting simulated deformations best fit the mesh deformed by the vision data. More formally, we minimize, we respect to $\mathbf{f}^{op}$, the least square error e_{force} between the deformations sensed through registration $\{\mathbf{x}_i^{vision}\}_{i=1}^{n_X}$ and the simulated deformations $\{\mathbf{x}_i^{sim}\}_{i=1}^{n_X}$, based on the interaction model.

$$e_{force}(\mathbf{f}^{op}) = \sum_{i}^{n_X} (\mathbf{x}_i^{vision} - \mathbf{x}_i^{sim}(\mathbf{f}^{op}))^2 \qquad (8)$$

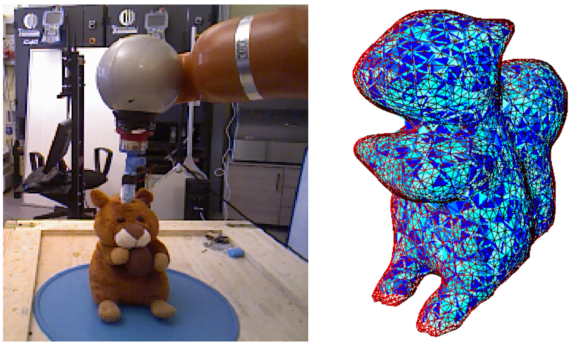

Figure 2: Left: The experimental set-up, with the tool mounted on the robotic arm equipped with a force sensor, compressing the object. Right: Surface triangular (in red) and volumetric tetrahedral mesh (in blue) of the stuffed toy.

The derivation of e_{force} given the full interaction model is a non-trivial task which requires the inversion of the model. Instead, since we aim at performing a quite global process without any strong guess on this force, we use a Nelder-Mead optimization framework to minimize e_{force} with respect to $\mathbf{f}^{op} = \left[f_x^{op} f_y^{op} f_z^{op}\right]^T$. In practice, in order to compute e_{force} for a given force $\mathbf{f}^{op}$, we start from the deformed state of the mesh, following registration. We then substitute all the external forces due to the point cloud data by $\mathbf{f}^{op}$ on the known vertex in contact with the operator. A simulation is evolved based on this force and the interaction model. After a few iterations in the simulation process, e_{force} is computed. It measures the ability of $\mathbf{f}^{op}$ to reproduce the actions of the forces on the object provided by vision.

6 EXPERIMENTAL RESULTS

The results presented here involve a deformable object, a stuffed toy undergoing a compression deformation effort applied by a tool fixed on the end-effector of a Kuka LWR arm, equipped with a force sensor at the wrist (see Fig. 2). The point clouds of the investigated scenes are acquired using a calibrated RGB-D camera Asus Xtion, 320 × 240 RGB and depth images being processed. For both the estimation of the elasticity parameters and the applied contact compression force, we process the data of a single RGB-D camera, taken at static equilibrium.

To build the deformation model of the stuffed toy, a surface mesh of the undeformed object was reconstructed offline using an RGB-D based dense 3D reconstruction technique (Newcombe et al., 2011), by flying around the object with the Xtion sensor. We then manually segment the part of scene featuring the object. Finally, some remeshing and smoothing procedures are performed with a modeling engine in order to get a fair, closed and clean surface mesh of the object.

The volumetric tetrahedral mesh was generated by carrying out a 3D Delaunay triangulation on the surface mesh, with the CGAL library[2]. As a compromise between modeling accuracy and real-time constraints, we have generated a volumetric mesh with 951 vertices and 5015 tetrahedral elements (see Fig. 2). As an approximation, we assume the isotropy of the material of the stuffed toy to apply the deformation model described in Sect. 2.1.

For modeling, we have employed the Simulation Open Framework Architecture (SOFA) simulator (Faure et al., 2012), which enables to deal with various physical models and to evolve simulations in real-time. In terms of hardware, a standard laptop with an NVIDIA GeForce 720M graphic card has been used, along with a 2.4GHz Intel Core i7 CPU.

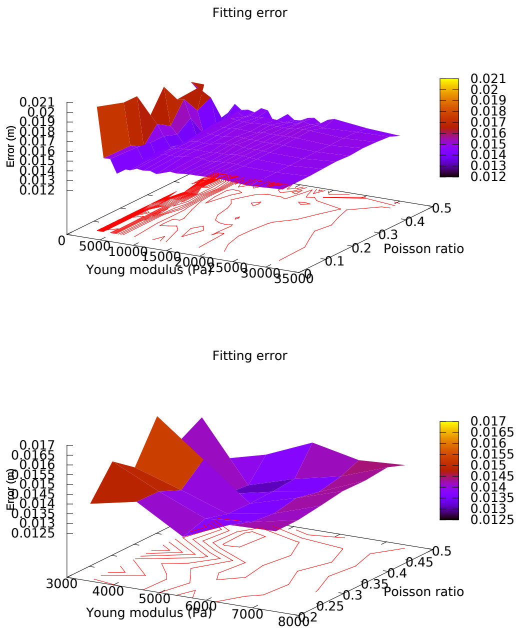

Figure 3: Top: Fitting error with respect to the elasticity parameters. Bottom: Closer view around the global minimum

6.1 Elastic Parameters Estimation

For the estimation of the elastic parameters, we first measure the contact force exerted by the tool mounted on the robotic arm to compress the object, giving a value of $\mathbf{f}^{op}_{mech} = [0.17 \;\; 1.125 \;\; 4.006]^T$. Due to the particular shape of the considered object, the application of this pointwise contact force in simulation may result in the loss of the static equilibrium. For this reason, we constrain the system by fixing the position of some vertices on the lower part of the shape, close to the contact area with the flat surface. In this way the object may not get bent excessively or turned over and its base remains quite rigidly attached to the flat contact surface.

Following the Nelder-Mead algorithm basic implementation and the parameter space for (E, ν) being of dimension 2, 3 candidate samples will be sorted after each iteration of the optimization, while performing the reflection, expansion, contraction and shrinking steps, providing a best, a good and a worst candidate. We also integrate the specific boundaries for both E and ν in the process, in the sense that inequalities $E > 0$ and $0 < \nu < 0.5$ should be preserved during the different steps. If an inequality is violated, E or ν is reset slightly below or above.

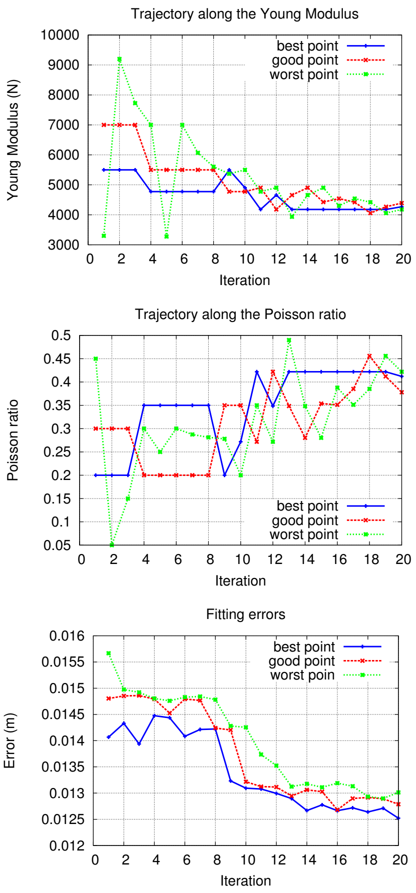

Figure 4: Nelder-Mead process for elasticity parameters estimation for the first initial configuration.

We have tested our parameters estimation technique with two different initial configurations. In

[2] http://www.cgal.org

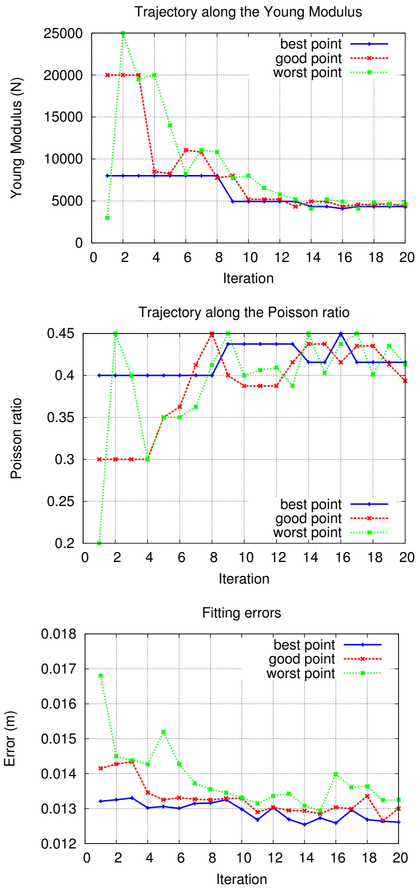

Figure 5: Nelder-Mead process for elasticity parameters estimation for the second initial configuration.

Fig. 4 and 5 we can observe for these two configurations the trajectories of the 3 sorted candidates, along E and ν throughout the iterations of the Nelder-Mead process. The figures show also the fitting errors for the 3 candidates after each iteration. In the first case the initial values are quite far from the actual estimated one, stressing out the robustness of the estimation with respect to coarse initial guesses, while, in the second configuration, the process starts closer to the solution.

For both configurations convergence is achieved respectively towards $(E,\nu) = (4268.65Pa, 0.412031)$ and $(E,\nu) = (4328.12Pa, 0.415625)$. The fitting error being prone to local minima, convergence may be reached after a certain number of iterations, around 8 in the first case and around 11, despite its closer initial values. On the plot of the fitting error in Fig. 3, it can be noticed that the non-convexity can be especially observable for the ν parameter, along which the error is quite flat, resulting in some local minima.

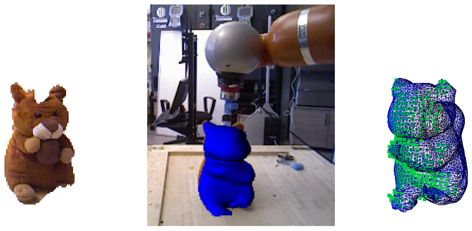

(a) (b) (c)

Figure 6: Registration process, with: (a) Preliminary segmentation, (b) Fitting result between the mesh and the segmented point cloud, (c) Registered mesh reprojected in the image.

6.2 Contact Force Estimation

With the aim of testing the operator contact force estimation based on the vision tracking system, we first proceed by setting the material parameters of the deformation models used in the vision system (here we use $(E,\nu) = (4268.65Pa, 0.412031)$). The result of the registration process can be observed in Fig. 6.

Let us remind that for each evaluation of the error function, the registered mesh is relaxed from the forces exerted by vision while applying the point wise contact force to evaluate on the known vertex. Fixing vertices as boundary conditions to constraint the simulation is not necessary since we measure here the ability of this force to keep the static equilibrium already reached by the action of the vision forces. The parameter space being of dimension 3, there will be 4 samples to sort after each iteration, the best, the worst and two intermediate ones. Two different initial configurations are tested here, starting respectively quite far, without any particular guess on the intensity and direction of the force, and close to the actual value of the force given by the sensor $\mathbf{f}^{op}_{mech} = [0.17 \ \ 1.125 \ \ 4.006]^T$. Figs. 7 and 8 show in both cases the trajectories of the four candidates for the estimate of the contact force $\mathbf{f}^{op}$, along X, Y and Z, and the corresponding fitting errors. In both cases, the algorithm converges respectively towards a force $\mathbf{f}^{op} = [0.618 \ \ 0.0687929 \ \ 3.54801]^T$ and $\mathbf{f}^{op} = [-0.462414 \ \ 0.247626 \ \ 3.71292]^T$, which are relatively close to the value sensed by the force sensor mounted on the robot, thus validating our whole model. Convergence is of course reached much faster in the second case.

7 DISCUSSION

The proposed framework consists in: 1) estimating the material parameters based on a known exerted force, in order to develop a deformation model; 2)

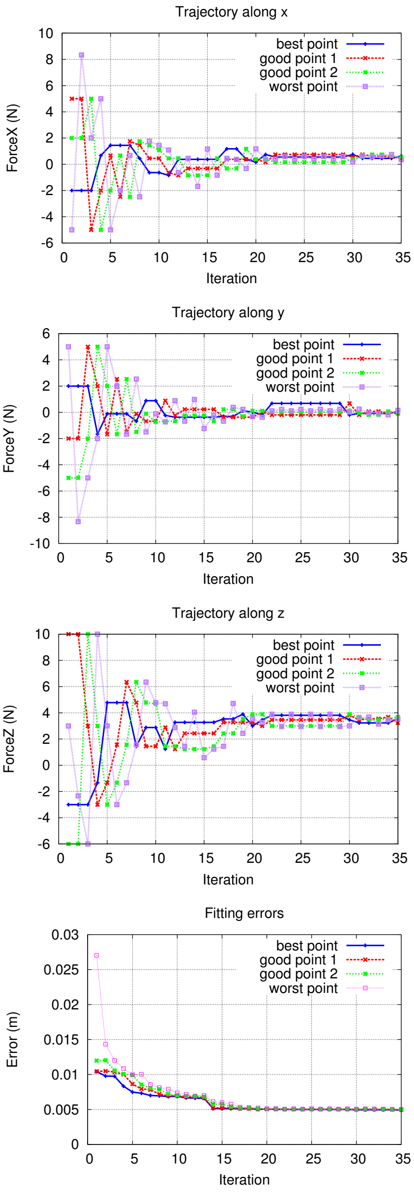

Figure 7: Nelder-Mead process for force estimation, for the first initial configuration.

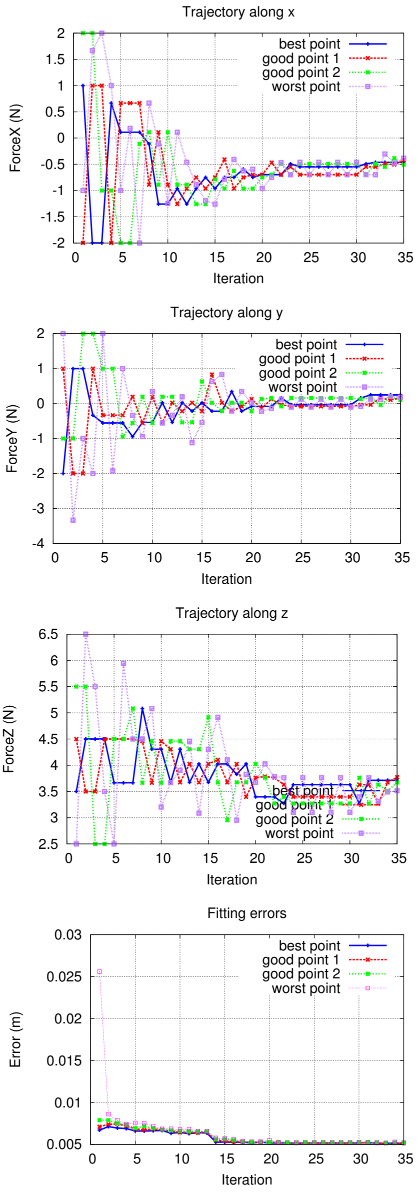

Figure 8: Nelder-Mead process for force estimation, for the second initial configuration.

estimating the force based on the known deformation model and on a registration technique that allows to measure deformations. The results presented in this paper are promising, but several issues shall be discussed.

7.1 Deformation capture set-up

Our imaging set-up is based on a single Asus Xtion RGB-D sensor, providing in quite low resolution, partial and noisy point cloud data around the object. It results in a non-convex shapes for the fitting error function in the elasticity estimation process, especially with respect to ν, or in registration errors.

A more sophisticated set-up to capture deformations, such as the one proposed in (Wang et al., 2015), with a set of RGB-D sensors at different viewpoint, would give more accurate results for the estimation of both the mechanical parameters and the contact force.

7.2 Interaction capture

In this work we assume the contact point between the object and the operator to be known, as well as the contact between the object and the underlying flat surface. A further development of our approach would be the design of a vision system able to capture the interaction between the object and its interacting environment: the manipulation tool, the table etc... enabling the detection of contact points, some useful priors for the segmentation and registration of the different entities.

7.3 Efficient inversion of the FEM

In the estimation of the force exerted by the operator, we use a gradient-free Nelder-Mead optimization method. It has the advantage of being quite easy to implement and robust to a coarse initialization, it is however quite slow to run. Indeed for force estimation, each evaluation of the error function requires at least 5 successive simulations to obtain a reliable error with respect to deformations of the registration process. An iteration in the Nelder-Mead algorithm requires in this case 7 evaluations, so around 350*ms*, given that one simulation takes around 10*ms*, making the process quite far from being real-time if considering a stream a successive RGB-D data. A possible improvement would be to investigate an efficient inversion of the full interaction model and some local optimization techniques such as quadratic programming, as proposed by (Largilliere et al., 2015).

7.4 Using dynamics towards deformation and force tracking

Our system is designed for the static case, for which deformations have reached a static equilibrium. It could be adapted to a dynamic case by benefiting from a measure, through vision, of the kinematics of the object or of interacting entities. Hence, based on Lagrangian dynamics, the system could track on-line both the deformations and the force.

8 CONCLUSION

In this work we have designed a system able to recover a single contact force exerted on a deformable object by resorting to an external vision and registration system and by fitting simulated deformations with the observed ones. This is achieved by taking advantage of a physically realistic deformation model based on an FEM approach, and by employing a basic interaction model with the manipulator and the environment, proposing here a simple manipulation scenario. The deformation model requires two mechanical parameters, the Young Modulus and the Poisson ratio, which we initially estimate, also by fitting simulated deformations with the point cloud given by an RGB-D sensor. The fully determined elastic model then feeds the registration system and the simulator, which are matched with respect to the contact force. We address these two optimization problems using gradient-free Nelder-Mead methods. Some promising results have been obtained on a simple case of single applied compression force on a known contact point, at static equilibrium. Future works would aim at extending the proposed approach to the dynamic case, and to benefit from the vision-based capture of the interactions.

ACKNOWLEDGEMENTS

This research has been partially funded by the EC Seventh Framework Programme (FP7) within RoDyMan project 320992 and by the national grant MUSHA.

REFERENCES

Ballan, L., Taneja, A., Gall, J., Van Gool, L., and Pollefeys, M. (2012). Motion capture of hands in action using discriminative salient points. In *European Conference on Computer Vision*, pages 640–653.

Brubaker, M. A., Sigal, L., and Fleet, D. J. (2009). Estimating contact dynamics. In *IEEE International Conference on Computer Vision*, pages 2389–2396.

Chen, Y. and Medioni, G. (1992). Object modelling by registration of multiple range images. *Image and vision computing*, 10(3):145–155.

Cirillo, A., Ficuciello, F., Natale, C., and Pirozzi, S., V. L. (2015). A conformable force/tactile skin for physical human/robot interaction. *IEEE Robotics and Automation Letters*, 1:41–48.

Cook, R. D. (1994). *Finite element modeling for stress analysis*. Wiley.

Dahiya, R. S., Metta, G., Valle, M., and Sandini, G. (2010). Tactile sensing–from humans to humanoids. *IEEE Transactions on Robotics*, 26:1–20.

Essahbi, N., Bouzgarrou, B., and Gogu, G. (2015). Soft material modeling for robotic task formulation and control in the muscle separation process. *Robotics and Computer-Integrated Manufacturing*, 32:37–53.

Etzmuß, O., Keckeisen, M., and Straßer, W. (2003). A fast finite element solution for cloth modelling. In *IEEE Pacific Conference on Computer Graphics and Applications*, pages 244–251.

Faure, F., Duriez, C., Delingette, H., Allard, J., Gilles, B., Marchesseau, S., Talbot, H., Courtecuisse, H., Bousquet, G., Peterlik, I., et al. (2012). Sofa: A multimodel framework for interactive physical simulation. In *Soft Tissue Biomechanical Modeling for Computer Assisted Surgery*, pages 283–321. Springer.

Fazioli, F., Ficuciello, F., Fontanelli, G., Siciliano, B., and Villani, V. (2016). Implementation of a soft-rigid collision detection algorithm in an open-source engine for surgical realistic simulation. In *IEEE Int. Conf. on Robotics and Biomimetics, ROBIO'2016*, pages 2204–2208.

Ficuciello, F., Carloni, R., Visser, L., and Stramigioli, S. (2010). Port-hamiltonian modeling for soft-finger manipulation. In *IEEE Int. Conf. on Intelligent Robots and Systems, IROS'2010*, page 42814286.

Frank, B., Schmedding, R., Stachniss, C., Teschner, M., and Burgard, W. (2010). Learning the elasticity parameters of deformable objects with a manipulation robot. In *IEEE/RSJ International Conference on Intelligent Robots and Systems*, pages 1877–1883.

Grieve, T. R., Hollerbach, J. M., and Mascaro, S. A. (2013). Force prediction by fingernail imaging using active appearance models. In *World Haptics Conference*, pages 181–186.

Hristu, D., Ferrier, N., and Brockett, R. W. (2000). The performance of a deformable-membrane tactile sensor: basic results on geometrically-defined tasks. In *IEEE International Conference on Robotics and Automation*, pages 508–513.

Kyriazis, N. and Argyros, A. (2013). Physically plausible 3d scene tracking: The single actor hypothesis. In *IEEE Conference on Computer Vision and Pattern Recognition*, pages 9–16.

Largilliere, F., Verona, V., Coevoet, E., Sanz-Lopez, M., Dequidt, J., and Duriez, C. (2015). Real-time control of soft-robots using asynchronous finite element modeling. In *IEEE International Conference on Robotics and Automation*, pages 2550–2555.

Mascaro, S. A. and Asada, H. H. (2001). Photoplethysmograph fingernail sensors for measuring finger forces without haptic obstruction. *IEEE Transactions on Robotics and Automation*, 17:698–708.

Müller, M. and Gross, M. (2004). Interactive virtual materials. In *Graphics Interface*, pages 239–246.

Nelder, J. and Mead, R. (1965). A simplex method for function minimization. *The Computer Journal*, 7(4):308–313.

Nesme, M., Payan, Y., and Faure, F. Efficient, physically plausible finite elements. In *Eurographics*, pages 77–80.

Newcombe, R. A., Davison, A. J., Izadi, S., Kohli, P., Hilliges, O., Shotton, J., Molyneaux, D., Hodges, S., Kim, D., and Fitzgibbon, A. (2011). Kinectfusion: Real-time dense surface mapping and tracking. In *IEEE International Symposium on Mixed and Augmented Reality*, pages 127–136.

Oikonomidis, I., Kyriazis, N., and Argyros, A. A. (2011). Full dof tracking of a hand interacting with an object by modeling occlusions and physical constraints. In *IEEE International Conference on Computer Vision*, pages 2088–2095.

Petit, A., Lippiello, V., Fontanelli, G. A., and Siciliano, B. (2017). Tracking elastic deformable objects with an RGB-D sensor for a pizza chef robot. *Robotics and Autonomous Systems*, 88:187–201.

Petit, A., Lippiello, V., and Siciliano, B. (2015a). Real-time tracking of 3D elastic objects with an RGB-D sensor. In *IEEE/RSJ International Conference on Intelligent Robots and Systems*, pages 3914–3921.

Petit, A., Lippiello, V., and Siciliano, B. (2015b). Tracking fractures of deformable objects in real-time with an RGB-D sensor. In *IEEE International Conference on 3D Vision*, pages 632–639.

Pham, T.-H., Kheddar, A., Qammaz, A., and Argyros, A. A. (2015). Towards force sensing from vision: Observing hand-object interactions to infer manipulation forces. In *IEEE Conference on Computer Vision and Pattern Recognition*, pages 2810–2819.

Sato, K., Kamiyama, K., Kawakami, N., and Tachi, S. (2010). Finger-shaped gelforce: sensor for measuring surface traction fields for robotic hand. *IEEE Transactions on Haptics*, 3:37–47.

Siciliano, B. and Khatib, O. (2008). *Springer handbook of robotics*. Springer Science & Business Media.

Sun, M., Su, H., Savarese, S., and Fei-Fei, L. (2009). A multi-view probabilistic model for 3d object classes. In *IEEE Conference on Computer Vision and Pattern Recognition*, pages 1247–1254.

Sun, Y., Hollerbach, J. M., and Mascaro, S. A. (2008). Predicting fingertip forces by imaging coloration changes in the fingernail and surrounding skin. *IEEE Transactions on Biomedical Engineering*, 55:2363–2371.

Urban, S., Bayer, J., Osendorfer, C., Westling, G., Edin, B. B., and Van Der Smagt, P. (2013). Computing grip force and torque from finger nail images using gaussian processes. In *IEEE/RSJ International Conference on Intelligent Robots and Systems*, pages 4034–4039.

Wang, B., Wu, L., Yin, K., Ascher, U., Liu, L., and Huang, H. (2015). Deformation capture and modeling of soft objects. *ACM Transactions on Graphics*, 34:94.

Wang, Y., Min, J., Zhang, J., Liu, Y., Xu, F., Dai, Q., and Chai, J. (2013). Video-based hand manipulation capture through composite motion control. *ACM Transactions on Graphics*, 32:43.

Wettels, N., Fishel, J., Su, Z., Lin, C., and Loeb, G. (2009). Multi-modal synergistic tactile sensing. In *Workshop on Tactile Sensing in Humanoids, Tactile Sensors and Beyond, 9th IEEE-RAS International Conference on Humanoid Robots*.

Yousef, H., Boukallel, M., and Althoefer, K. (2011). Tactile sensing for dexterous in-hand manipulation in robotics. A review. *Sensors and Actuators A: Physical*, 167:171–187.

Yuan, W., Li, R., Srinivasan, M. A., and Adelson, E. H. (2015). Measurement of shear and slip with a gelsight tactile sensor. In *IEEE International Conference on Robotics and Automation*, pages 304–311.

Zhao, W., Zhang, J., Min, J., and Chai, J. (2013). Robust realtime physics-based motion control for human grasping. *ACM Transactions on Graphics*, 32:207.